Structural Character and Energetics of Tyrosyl Radical Formation by Electron/Proton Transfers of a Covalently Linked Histidine-Tyrosine: A Model for Cytochrome *c* Oxidase

Yuxiang Bu[†] and R. I. Cukier*

Department of Chemistry, Michigan State University, East Lansing, Michigan 48824-1322

Received: June 7, 2005; In Final Form: September 20, 2005

The structural, energetic, and electronic and IR spectroscopic properties for a model of the cross-linked histidine-tyrosine (His-Tyr) residues as found in cytochrome *c* oxidase (C*c*O) are investigated by ab initio methods. The formation of a His-Tyr radical is studied by two paths: proton release followed by electron release and vice versa. The energetics for the proton/electron releases of the Tyr depend modestly on the cross-linked His substituent and, more sensitively, on the charge of the cation attached to the imino N site of the His residue. Protonation of the imino N site significantly increases the electron ionization potential and decreases the proton dissociation energy, making them competitive processes. A positive charge placed at the imino N site, whose value is scanned from zero to one, shows a continuous increase in ionization potential and a decrease in proton dissociation energy, with the +1 limit agreeing well with the protonated imino N site result, indicating a dominant electrostatic effect. The charge populations and the spin density distributions of the His-Tyr model, the radical cation formed by electron ionization, the anion formed by proton dissociation, and the final His-Tyr radical depend sensitively on the substituents, implying a modulation role on the charge transfer between the phenol and imidazole rings, especially for the charged species. His-Tyr and protonated His-Tyr exhibit differences among their respective structural isomers with consequences on their IR absorptions. Small barriers between their pseudo-cis and pseudo-trans rotamers demonstrate the relative flexibility between the two rings, and these may facilitate proton release and charge transfer. The cation effect demonstrates that the cationized cross-linked His-Tyr should be the best candidate to mimic the covalently ring-linked histidine-tyrosine structure in C*c*O.

1. Introduction

Cytochrome *c* oxidase (C*c*O), the terminal enzyme of the respiratory chains of mitochondria and aerobic bacteria is a membrane-bound redox-driven proton pump.[1] Located in the inner mitochondrial membrane, it catalyzes the reduction of molecular oxygen to water and pumps protons across the membrane.[2−4] Electron transfer is coupled to proton translocation across the membrane, resulting in a proton and charge gradient that is then employed by the F_0F_1-ATPase to synthesize ATP. C*c*O contains two hemes, heme *a* and heme a_3, a dimeric copper center, Cu_A, and a mononuclear Cu_B. Heme a_3 is associated with the proximal Cu_B (∼4.5−5.0 Å to the Fe), defining the heme−copper binuclear center, where O_2 reduction takes place. Breakage of the O−O bond and its conversion to water requires four electrons and eight protons in the catalytic cycle for C*c*O. The O_2 reduction process may be divided into two distinct stages of oxidative and reductive half reactions. The former may be viewed as oxidation of the cofactors in which all four electrons are provided by the binuclear center, after O_2 is bound to the heme a_3 active site, while the latter may be viewed as the reduction of the binuclear center, in which the necessary four electrons come from Cu_A via heme *a*. In the first stage, since the cofactors only provide three electrons (two from heme a_3 and one from Cu_B), it has been suggested that the fourth electron comes from a proximal tyrosine that is oxidized to a neutral tyrosyl radical in an intermediate process.[5,6] Mutagenesis studies have also shown that this residue is crucial to enzyme function. Formation of the tyrosyl radical and reformation of tyrosine may be viewed as an electron transfer followed by proton transfer, or vice versa, or as a hydrogen-atom transfer. Which mechanism operates depends on the energetics of the steps involved and leads to intermediates with very different characteristics that are, in principle, amenable to detection by various spectroscopic methods.

The structures of C*c*O in its fully reduced and various oxidized states have been explored and characterized in detail. The features of the binuclear center are that the heme a_3 Fe is axially ligated to a histidine (His) residue and the Cu_B ion is ligated by three His residues. An unexpected feature of the binuclear site is a covalent linkage between one of the Cu_B His ligands and a tyrosine (Tyr) residue[7−9] (His^{240}-Tyr^{244}, in bovine heart C*c*O[7]), via the ortho site C of the Tyr^{244} residue and the amino N of the His^{240} residue. Buse et al. provided evidence for the existence and the character of this unusual structure in the active site of C*c*O on the basis of the protein chemical analysis.[10] Van der Donk and co-workers studied the functional role of the His-Tyr linkage in C*c*O using spectrophotometric titration methods on model compounds.[11] In view of the specificity of this unexpected linkage and its importance in the dioxygen reduction process, great efforts have been made in exploring the structural character and nature of this covalently linked system and in elucidating its role in regulating the redox reaction process (dioxygen reduction and the recovery process of the binuclear active center for the next catalytic cycle).[10−28] Tomson et al. recently performed direct IR detection of the

* Corresponding author. E-mail: cukier@cem.msu.edu.
[†] Permanent address: Institute of Theoretical Chemistry, Shandong University, Jinan 250100, China. E-mail: byx@sdu.edu.cn.

10.1021/jp053046t CCC: $30.25
Published on Web 10/25/2005

covalently ring-linked His-Tyr structure in the active site of the heme−copper oxidases using a synthetic analogue,[16] and some helpful spectroscopic signatures (a feature near 1546 cm^{-1}) related to the unique covalently linked structure were observed. In addition, others have reported syntheses of covalently linked imidazole−phenol structures[11,29] with the objective of producing synthetic mimics of the covalently linked His-Tyr structure in the oxidases. Among these synthetic modeling compounds, His and Tyr were modeled by imidazole/*p*-cresol,[11] His/phenol,[26] 4-methyl-imidazole-1-yl/*p*-cresol,[27] and other analogues,[22,25] and different structural and spectroscopic characters have been observed.

The discovery of the His-Tyr cross-link at the active site led to the proposal that Tyr may function as an electron[30] and a proton donor to the dioxygen bound to heme a_3,[14,31,32] thus facilitating the cleavage of the dioxygen bond. On the other hand, several groups have also speculated that the cross-linked Tyr might serve as a hydrogen-atom donor during the reduction of O_2.[14,31] Many investigations demonstrated that the feasibility of these functional roles critically depends on the perturbation of the physicochemical properties of Tyr as a result of the covalent bond to His. Although the details of the reduction mechanism are in debate, the prediction that Tyr will release a proton and an electron, becoming a radical in a certain intermediate stage, as the normal Tyr function in the relevant reduction processes, is reasonable and occurs in other redox enzymes.[33] As pointed out by Davies, the imidazole and phenol rings of His and Tyr residues are among the most susceptible side chains for the radical reactions of the protein amino acids.[34] The existence of a Tyr radical in the reaction of C*c*O with hydrogen peroxide was recently demonstrated by electron paramagnetic resonance (EPR).[13]

The Tyr^{244}-His^{240} cross-link (*Paracoccus* numbering) may also serve other roles. For example, Yoshikawa et al. suggested that the cross-linked tyrosine is deprotonated in the fully oxidized state of the enzyme.[7] Thus, the protonation of Tyr^{244} is required to prime the enzyme for catalysis. Namely, it has been proposed that two protons required to reduce the binuclear center to its fully reduced state (R state) are delivered to the binuclear center via Tyr^{244}, and one of the protons is used to protonate Tyr^{244} (in its recovery process) and, together with an incoming electron, prepare it for its role in O−O cleavage.[31] Clearly, the experimentally demonstrated existence of the tyrosine radical intermediate has at least revealed that Tyr^{244} not only releases an electron and a proton to the dioxygen moiety in the oxidative half reaction but also must get an electron and a proton from other places in the reductive half reaction. For the recovery process of Tyr from the radical, a more certain conclusion is that the required electron and proton come from different active sites or parts of the protein.

For the oxidative process of Tyr, the electron/proton transfer mechanism is still in debate. Although the released electron and proton are transferred to the terminal O of the dioxygen bound to the heme a_3 Fe center, the nature of the transferred species (electron + proton) is unknown. Is it a H-atom transfer, or is it a concerted or consecutive electron/proton transfer? If it is the latter, is it cooperative in the sense that, for example, if electron transfer occurs first, does it influence the proton transfer probability? Some clues can be obtained by inspection of the C*c*O structure.[7] For example, the terminal O is not directed toward the Tyr OH group, just after O_2 is bound to the heme a_3 Fe center, but rather toward the Cu_B center. This arrangement favors not only the reduction of O_2 by electron transfer from heme a_3 and Cu_B but also the binding of the terminal O to the Cu_B center, because O_2 may effectively couple with these two active metal centers. On the other hand, inspection also reveals that the distance between the H of Tyr OH and either O of O_2 is more than 4 Å. This long distance does not favor H-atom transfer, even if some water molecules exist in the pathway, because a hydrated H-atom transfer is much less probable than proton transfer along hydrogen-bonded water molecules. Certainly, as an approach, the just bound O_2 may be proposed to point to the H of the Tyr OH. However, electron transfer from Cu_B to O_2 becomes unfavorable due to the long Cu···O distance and, also, the H-atom transfer distance is still much longer than the most optimal one. Even if the H atom may transfer to the terminal O, the O−O cleavage should generate an OH radical, and then, the terminal O must move to the Cu_B center as an OH radical. However, to date, there is no experimental evidence for the formation of an OH radical. In addition, before a fourth electron transfers to the O_2 moiety, O−O cleavage is energetically unfavorable even if present as HOO···Fe (heme). These comments indicate that the possibility of direct H-atom transfer from Tyr to the terminal O is questionable. Thus, for both the oxidation and reduction of the Tyr moiety, the species involved are an electron and a proton, instead of a H atom, though, of course, the electron transfer may be coupled to the proton release.

In this work, we computationally probe the electron/proton transfer mechanism of cross-linked His-Tyr models and some of their derivatives by evaluating the electron ionization potential (IP)/electron affinity (EA) and the proton dissociation energy (PD)/proton affinity (PA). How the cross-linkage affects the relevant energy quantities, and the structural and spectral properties, is of interest and complements and extends several recent works that focused on cross-linked His-Tyr synthetic models and spectra.[11,22,25−27] Of course, the surrounding metals, cofactors, and residues also can have important effects on these properties, but the starting point should be with the cross-linked His-Tyr and its derivatives. While the surroundings will influence the priority of IP/EA and PD/PA from the cross-linked His-Tyr models, what must first be assessed is the electronic structure of these models. An important effect omitted in all previous investigations is that the His is ligated to Cu_B, a cation whose charge varies between +1 and +2 in the course of the O_2 chemistry. A cation coupling effect should play a profound role in modulating the electron/proton release or acceptance. The energetics and the relative priority of the two transfer processes have never been discussed, and the structure and spectroscopic characters of possible intermediates (such as the cation radical after ionization of Tyr in the oxidization process or after protonation of Tyr radical in the recovery process and the anion after proton dissociation in the oxidization process or after electron capture in the recovery process) have not been explored. The role of the cross-linkage on these properties also is of interest. Thus, we will compare the relevant property changes of the Tyr moiety by introducing different substituents (such as methyl-imidazole or protonated methyl-imidazole groups) into the ortho site of Tyr and suggest a potential function of the Tyr moiety in the dioxygen reduction process based on our results.

The remainder of this paper is structured as follows: Section 2 briefly describes the computational method that is used. The structural character and analyses of properties for the cross-linked His-Tyr model and their derivatives, along with the substituent effects on the energetics of electron/proton release from the Tyr moiety, are presented in section 3. The biological

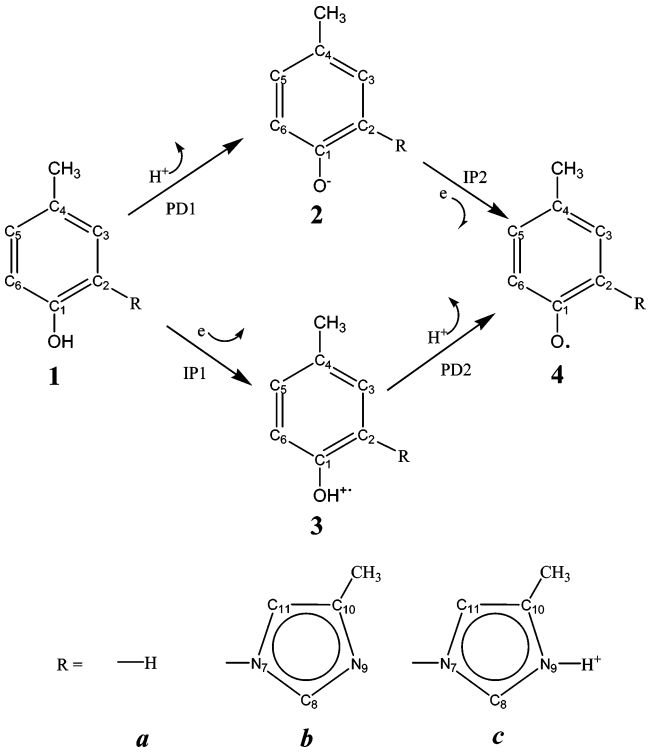

Figure 1. Schematic representation of various processes for the modeling tyrosine derivatives.

implications are discussed in section 4, and our concluding remarks are given in section 5.

2. Basic Considerations and Calculational Details

To establish a benchmark for comparison, several systems associated with a tyrosine residue are considered, as schematized in Figure 1. To be a valid cross-linked His-Tyr model, the effective compound needs to incorporate (a) imidazole and phenol rings linked by a covalent bond between the equivalent atoms to the His amino N and the Tyr *ortho*-C in His-Tyr and (b) aliphatic groups in the correct positions to mimic the His and Tyr side chain backbones in His-Tyr. The substitution at the correct position is a requirement because these aliphatic groups influence not only the IR spectroscopic features of the cross-linked structure but also its energy quantities and other electronic indexes. Thus, the backbone effect of the tyrosine is modeled by *p*-cresol or 4-methyl-phenol (hereafter called modeling Tyr). Since the explicit changes mainly occur in the OH group of Tyr, a new designation, Tyr-OH, is used to emphasize the changes of the modeling Tyr moiety that occur by removing or adding an electron/proton in the redox processes. To model the His cross-linked Tyr, a simplified His (4-methyl-imidazole-1-yl, the modeling His) is introduced to the *ortho*-C site of *p*-cresol, forming 4-methyl-2-(4-methyl-imidazole-1-yl)-phenol, and represented as His-Tyr-OH, that will also be referred to as a modeling cross-linked Tyr. The design of these modeling Tyr compounds is also motivated by several synthetic models and the associated spectroscopic analyses.[11,16,22,25−27,29] Similarly, to include the cation effect arising from the Cu_B center, a proton is used to protonate the imino N site of His-Tyr-OH, forming a H^+His-Tyr-OH species, another modeling cross-linked Tyr. In parallel, a point charge model is also employed in which a variable-magnitude positive point charge is placed at the position of the proton used to protonate the imino N site that directly ligates to the Cu_B center, to mimic the positive charge effect arising from the Cu_B center.

For the above systems, the ionization potential (IP) and the proton dissociation energy (PD) are theoretically determined at the B3LYP/6-311++G** level. Two schemes for electron and proton release of the Tyr moiety and the His-cross-linked Tyr derivatives, to form the corresponding radical products, are shown in Figure 1. Electron ionization forms a cation radical intermediate (IP1) and proton dissociation (PD2) produces the neutral radical, or proton dissociation (PD1) forms an anion intermediate and electron ionization (IP2) forms the neutral radical. These different schemes express two different electron and proton transfer modes of the Tyr moiety during the dioxygen reduction process. The corresponding recovery process of the Tyr radical to the original Tyr form for the next catalytic cycle can be easily understood from Figure 1 in which the relevant energy quantities should be referred to the electron affinities and proton affinities, the same values as the corresponding IP/PD but with opposite sign. Therefore, it is suitable to use IP/PD to describe the ability of releasing an electron and proton for the Tyr moiety or that of binding an electron and proton for the Tyr radical.

From the above designed schemes, for each modeling Tyr series, four species have been investigated: the reactant (the neutral modeling Tyr moiety), two possible intermediates (the anion or the cation radical), and the product (the neutral modeling Tyr moiety radical). In addition to the energy determinations, the infrared spectrum, Mulliken charge populations, and spin density distributions of all possible species have also been determined at the same level of theory to provide information for further experimental measurements.

Additionally, two points should also be noted: (1) the average errors of the energy quantities relevant to our present study (ionization potential, electron affinity, and proton affinity) of the B3LYP functional have been estimated using the extended G3 benchmark set[35] and are, respectively, 4.15, 2.83, and 1.43 kcal/mol (B3LYP/6-311+(3df,2p)//B3LYP/6-31G(d) functional). Together with many other calculations using the B3LYP method, these results fully demonstrate that it is a reliable tool to determine the energies and structural and spectroscopic properties for the systems considered here. (2) The effect of the basis set superposition error (BSSE) on the PD/PA energies and the zero-point vibrational energy (ZPVE) corrections on IP/EA and PD/PA should generally be taken into account. However, our recent investigations regarding proton release from imidazole[36] indicate that although these corrections could improve these energy quantities, they are at most 4 kcal/mol, and did not change the relative regularity among them, because the contributions from these corrections are significantly smaller than the corresponding uncorrected values. Therefore, in this work, the BSSE and ZPVE corrections are examined only for the energy quantities of the isolated modeling Tyr, for the validation of our preliminary analysis, and no corrections are applied to all other energy quantities. All calculations are performed using the Gaussian 03 program package.[37]

3. Results

Phenol and Modeling Tyrosine Derivatives. Phenol (PhOH) and its derivatives are important antioxidants in living organisms and many commercial products.[38] Phenolic antioxidants inhibit auto-oxidation by providing a hydrogen atom that is easily abstracted to form the corresponding relatively stable phenoxy radical. The oxidation can be viewed as an electron and proton transfer, and these steps are mainly determined by the phenolic IP and PD energies, though the environment can also influence these energetics. Since most of the changes induced by the

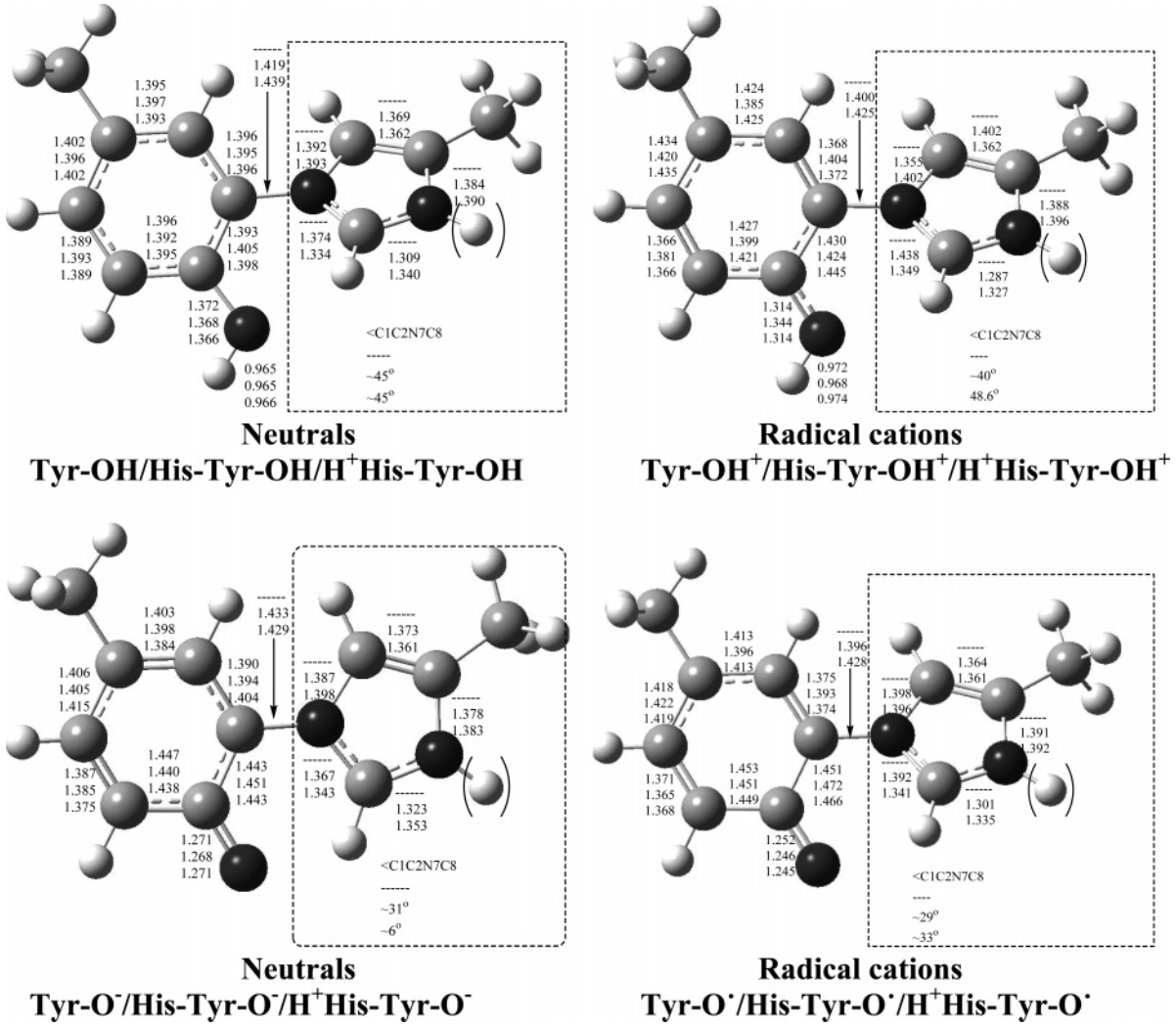

Figure 2. Molecular geometries and the corresponding main geometrical parameters for three modeling tyrosine series (Tyr-OH, His-Tyr-OH, and H^+His-Tyr-OH) with four species (neutral, radical cation, anion, and radical) for the pseudo-cis rotamers. The data from top to bottom for each geometrical parameter are referred to as the Tyr-OH, His-Tyr-OH, and H^+His-Tyr-OH derivative series, respectively, determined at the B3LYP/6-311+G* level. For each formalism, the fragments out of the dot-square boxes denote Tyr-OH derivatives. The H^+His-Tyr-OH derivative series can be formed by replacing the ortho(C2) site H by the fragments in the dot-square box, while the corresponding His-Tyr-OH derivative series may be formed by deleting the bracketed H linked to the other N site. The atomic numbering is the same as that in Figure 1

electron/proton transfers lie mainly in the hydroxyl group, the properties of the C−OH and O−H bonds are of interest.

At the B3LYP/6-311+G* level, the PhOH calculated C−O and O−H bond lengths are 1.370 and 0.965 Å, and the corresponding infrared stretching frequencies are 1275.2 and 3789.6 cm^{-1}, respectively. Recent works,[39,40] using the same theoretical method but with the slightly smaller DZP basis sets, obtained C−O and O−H bond lengths of 1.374 Å/1.373 Å and 0.968 Å/0.968 Å, respectively. These calculated results agree well with each other, and they are also very close to the experimental geometries.[41] Their calculated IR vibrational frequencies are 1288 and 3845 cm^{-1},[40] respectively, also being in good agreement with ours and the corresponding experimental values (1262 cm^{-1},[42] 3657 cm^{-1} [43]). Our optimized geometrical parameters and IR frequencies of the phenol radical cation ($PhOH^+$) and phenoxy radical ($PhO^•$) are 1.310 Å/1391 cm^{-1} (C−O) and 0.973 Å/3692 cm^{-1} (O−H) for $PhOH^+$ and 1.253 Å/1421 cm^{-1} (C−O) for the $PhO^•$ radical, respectively, in good agreement with other theoretical values (1.316 Å/1504 cm^{-1} (C−O) and 0.977 Å/3732 cm^{-1} (O−H) for $PhOH^+$ and 1.261 Å/1410 cm^{-1} (C−O) for $PhO^•$)[39,40] and the experimental values (1398 cm^{-1} (C−O) for $PhO^•$ [44]). Good agreement among them, together with comparison with other experimental values,[45,46] fully confirms the accuracy of the method (B3LYP/6-311+G*) used here. Similarly, we have also determined the relevant properties of the phenoxy anion (PhO^-). The C−O bond length is optimized to be 1.269 Å, and the IR frequency is 1539 cm^{-1}. Comparison among the four energies corresponding to the transformations in Figure 1, as applied to PhOH, indicates that although IP2 = 50.0 kcal/mol is the smallest, PhO^- has the largest proton dissociation energy (PD1 = 349.6 kcal/mol) and, therefore, this process is energetically unfavorable unless a very strong base is used as the proton acceptor. If so, the formed PhO^- may be easily converted into a $PhO^•$ radical. However, for the $PhOH^+$ mechanism, IP1 (191.1 kcal/mol) is significantly smaller than PD1. Therefore, the $PhOH^+$ pathway is both thermodynamically and kinetically more favorable to produce $PhO^•$ than the PhO^- pathway.

To model tyrosine, a methyl ($-CH_3$) is attached to the para site of the phenol ring, forming the 4-methyl-phenol (*p*-cresol) derivative. Here, we use the symbols Tyr-OH, Tyr-OH^+, Tyr-O^-, and Tyr-$O^•$ to denote the modeling tyrosine derivatives to emphasize the changes of the modeling Tyr active group −OH. The optimized structures and the main geometrical parameters are shown in Figure 2. A comparison of the four phenol-based derivatives with the corresponding methyl-substituted derivatives

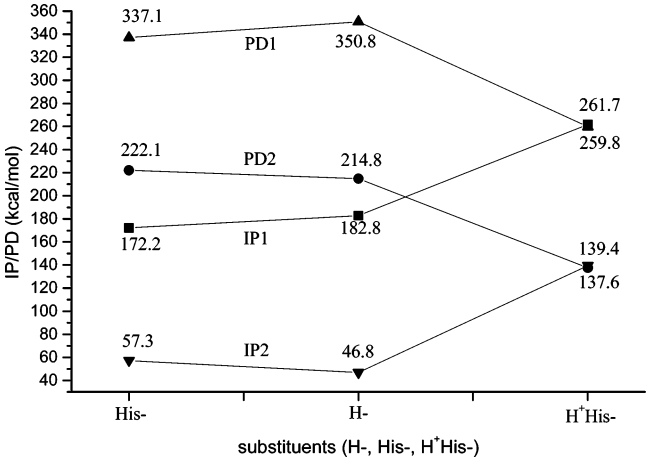

Figure 3. Dependencies of four energy quantities (IP1, PD2, PD1, and IP2) of Tyr moieties on the substituents (H-, His-, and H^+His-).

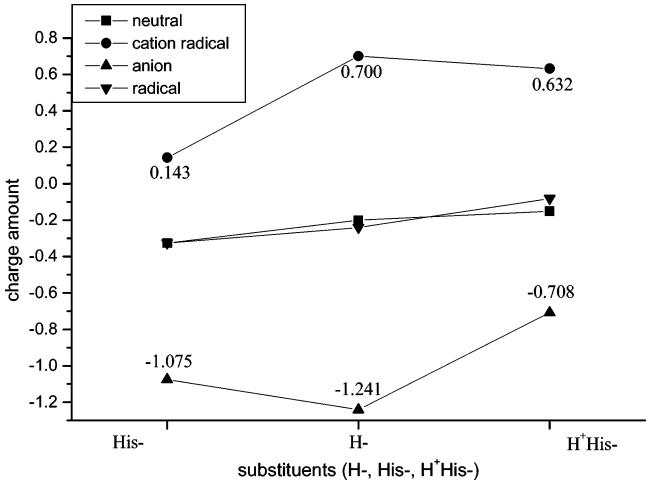

Figure 4. Dependencies of Mulliken charge populations over the Tyr moieties on the substituents (H-, His-, and H^+His-). The charge populations used here were obtained by summing the charges of all atoms belonging to the Tyr moiety.

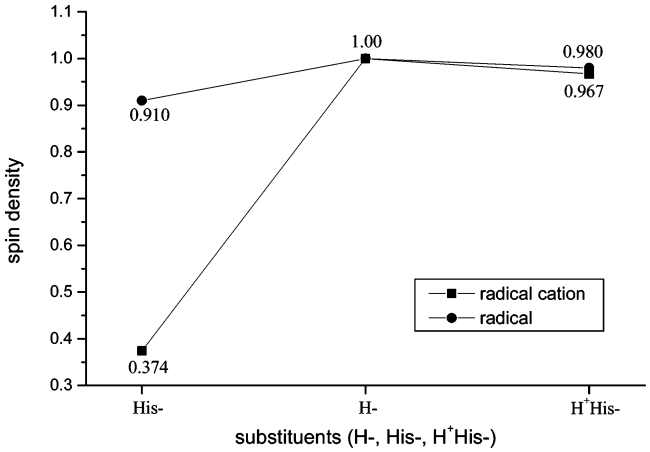

Figure 5. Dependencies of the total Mulliken spin densities over the Tyr moieties on the substituents (H-, His-, and H^+His-). The spin densities used here were obtained by summing the spin densities of all atoms belonging to the Tyr moiety.

indicates that no large geometric changes occur, but some energy quantities do change. Interestingly, the energies in the PhO^- pathway are minimally affected. Furthermore, the IR spectral characteristics of the Tyr-OH derivative series also are similar to the phenol derivative series. To examine the effect of a large substituent, we also consider the actual tyrosine amino acid. The results indicate that the geometries and IR frequencies hardly change, but both IP1 and PD1 slightly decrease and PD2 and IP2 slightly increase by a few kilocalories per mole. We have also examined the substituent effect via calculating the hydrogen-atom dissociation energies for PhOH, modeling tyrosine. The energy changes caused by increasing substituent size are negligible. These analyses show that it is reasonable to use a methyl group to mimic the substituent effect, since extension of the models beyond 4-methyl-phenol can be expected to have little influence on the calculated values. Therefore, 4-methyl-phenol derivatives are used as the modeling Tyr derivatives in the following discussions and will be referred to as Tyr-OH, Tyr-OH^+, Tyr-O^-, and Tyr-$O^\bullet$, respectively.

Figure 1 outlines two oxidation schemes for the modeling Tyr where one forms an anion intermediate, while the other yields a cation radical intermediate; thus, we will call these two different mechanisms the anion mechanism and the radical mechanism, respectively. Geometrically, there are significant changes for some parameters upon electron transfer. The key two are the C−O and O−H bonds. The C−O bond (1.372 Å) is significantly shortened by ∼0.6 Å, tending to but still longer (1.314 Å) than a normal double bond, while the O−H bond is slightly elongated by 0.07 Å. Because the electron ionization or transfer strengthens the C−O bond and weakens the O−H bond, just from this aspect, it can be predicted that the radical intermediate hydroxyl proton may be more easily released. Similarly, for the phenyl ring, the main change is that the basically averaged C−C bonds (1.389−1.402 Å) become inequivalent in part; namely, the C2−C3/C5−C6 bonds are reduced by ∼0.03 Å, and the C−C bonds made up of the C atoms that connect with the O center or $-CH_3$ group, respectively, are elongated by ∼0.03 Å. The delocalization of the conjugated π system is considerably broken, decreasing the aromatic stability of the system.

Comparison of the Mulliken charge population (displayed in Figure 4) and Mulliken spin density (displayed in Figure 5) can distinguish the changing details of the electronic densities. For the −OH group, the electronic density goes down by 0.22*e* upon single electron ionization, becoming positively charged. For the phenyl C ring, the positive charge goes up from 0.49*e* to 1.045*e*, and the methyl loses about 0.23*e*, indicating that the major change upon single electron ionization mainly lies in the phenyl ring. The spin density displayed in Figure 6 also reveals that 83% of the total spin density is over the ring, and it is mainly (67%) distributed over C1 and C4. The spin density over the O center is only 17%. Thus, the ionized electron is taken mainly from the ring, and the ionization greatly decreases its aromaticity, making the system more unstable. To make the system more stable requires electron density from the −OH group; however, the electron cloud is confined by the hydoxyl proton and cannot freely move to the ring. Therefore, the attraction of the ring for the electron over the −OH group becomes the driving force for the −OH proton release, making the proton more readily released. Upon proton release, the excess electron cloud over the O center may spontaneously transfer to the phenyl ring, increasing its aromaticity and stabilizing the system, mainly through a conjugation effect. That is, because of the attractive interaction of the ring for the electrons over the O center, the p orbital of the O center, together with the occupying electrons, interacts with the conjugated π bonding (Π_6^6), forming a larger conjugated π bonding system (Π_7^7) and increasing the aromaticity. As a result, upon the proton release, the C−O bond is significantly further shortened from 1.314 to 1.252 Å, close to the normal ketone C═O double bond (∼1.2 Å).

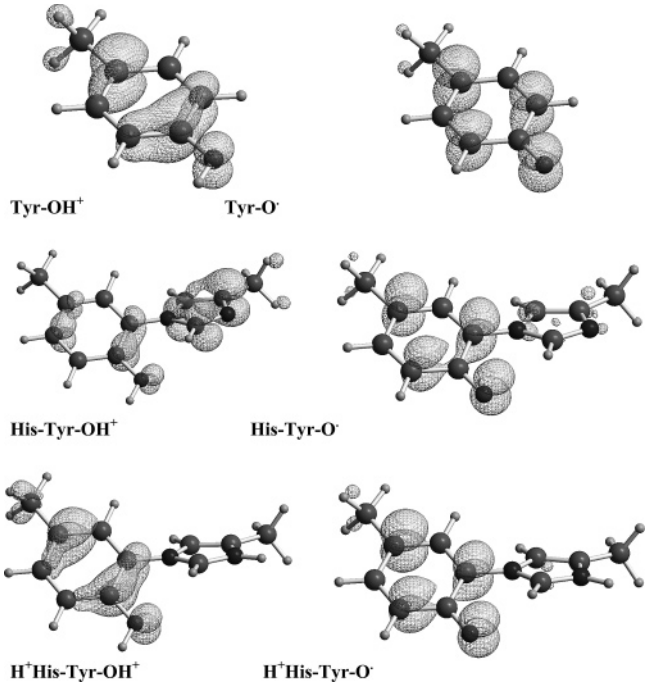

Figure 6. Spin density distribution contours for the radical cations and the radicals of three different systems with different substituents (H-, His-, and H^+His-). The isospin value is 0.002 au.

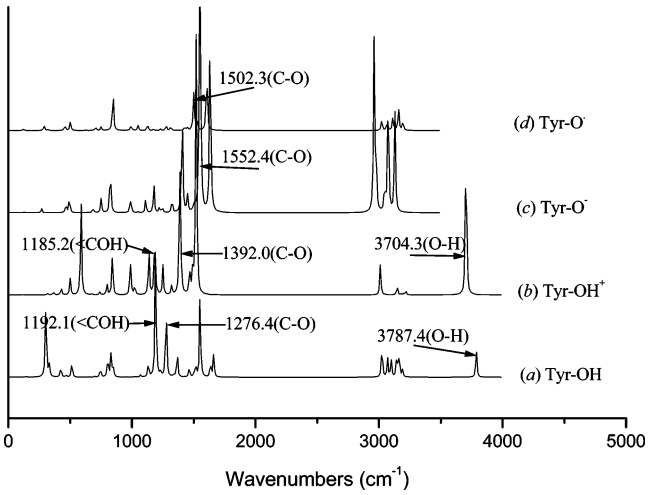

Figure 7. IR spectra of the Tyr-OH series derivatives and some special vibrational modes.

There is a distinct difference in the phenyl ring structure of Tyr-O• versus Tyr-OH. The geometrical changes result from an increase in the extent of conjugation between the O and the phenyl ring and the conjugation differences between Tyr-OH and Tyr-O•. In the latter, the conjugation of the O atom with the phenyl ring has strengthened the C−O bond. In addition, the electron density increase (0.34*e*) over the phenyl ring in Tyr-O• compared with that in Tyr-OH^+ also indicates the relative overall stability of two systems. Another interesting aspect is the change of spin density distribution (cf. Figure 6). The spin densities mainly distribute over O (0.40), *para*-/*ortho*-C (0.43, 0.30, 0.33) in the Tyr-O• radical, significantly different from those in Tyr-OH^+.

There are spectroscopic differences among the four modeling Tyr derivatives, and several particular vibrational modes can be assigned (cf. Figure 7). Upon electron ionization, the O−H stretching vibration is red-shifted by 83 cm^{-1} and the C−O stretching is blue-shifted by 116 cm^{-1}. The COH bending vibration is basically unchanged. Further, proton release of Tyr-OH^+ results in the C−O stretch being significantly blue-shifted by ∼116 cm^{-1}. These spectroscopic characteristics are in good agreement with the changes of geometries and charge population.

Turning now to the anion mechanism (see Figure 1), after proton transfer to form Tyr-O^-, the remaining negative charge diffuses into the conjugated phenyl ring, and 0.45*e* electron is transferred. The electron transfer and orbital coupling interaction result in the formation of a new large conjugated π bonding system, Π_7^8, which increases the C−O bonding but weakens the C1−C2/C1−C6 bonds. Of course, in a biological setting, the transferred proton may hydrogen-bond back the O center; thus, the geometries should fall between Tyr-OH and Tyr-O^-. Spectroscopically, the H−O stretching peak disappears, and the C−O stretching peak is blue-shifted compared to Tyr-OH and Tyr-OH^+, and even much more than that in Tyr-O•. Another point is the absence of an electron spin signal for this anion intermediate. This feature may be used to judge the actual electron/proton transfer mechanism. However, it should be noted that the anion intermediate has a denser electron cloud, increasing its susceptibility to oxidization (IP2 ∼47 kcal/mol), so that it may be short-lived and difficult to see in an experiment.

Covalently Linked Histidine-Tyrosine. The covalently linked model His-Tyr-OH defined in Figure 1 has geometrical parameters given in Figure 2 that show minor modifications in the phenol ring relative to the model Tyr-OH. The optimized C−O bond length in His-Tyr-OH is 1.368 Å, slightly shorter than that (1.372 Å) of Tyr-OH, while the corresponding O−H bond and all C−C bonds are almost equivalent. Similarly, the geometrical parameters in the His moiety are also very close to those in the free His molecule. The His moiety still keeps its planar character and aromaticity. The important C−N link bond is optimized to be 1.419 Å, implying a bond intermediate between a single and double bond, and is longer than all of the C−N bonds in the imidazole ring. With a dihedral C1C2N7C8 angle of ∼45°, the two rings (phenyl and imidazole) are not coplanar, which arises from the steric repulsion mainly between the O center and its neighboring C8−H moiety. The replacement of an ortho site H by the modeling histidine group leads to 0.13*e* electron transfer to the modeling Tyr moiety, indicating that the imidazole group is an electron donating group.

The optimizations also find another stable rotamer corresponding to an ∼90° rotation about the C−N bond. If their $-CH_3$ groups are selected as a reference, the former may be thought of as a pseudo-cis rotamer (with a dihedral angle of ∼45°), while the latter would be the pseudo-trans one (with a dihedral angle of ∼135°). The pseudo-cis rotamer is energetically more stable than the pseudo-trans one by only 0.07 kcal/mol at the B3LYP/6-311+G* level, and the geometrical parameters are essentially the same. The corresponding rotation barrier is ∼0.7 kcal/mol with a transition state where the two planes are basically normal to each other. In addition, there are also two other image isomers, also taken as the rotamers. The corresponding dihedral angles for them are ∼ −45° and ∼ −135°, respectively, and the rotation transition states correspond to the cis (dihedral angle 0°) and trans (dihedral angle 180°) coplanar structures. The rotation activation barrier for the cis species is ∼2.0 kcal/mol, while that for the trans species is ∼2.7 kcal/mol. These very low rotation barriers indicate that the cross-linked structure readily isomerizes.

Figure 8 displays the IR spectra for the His-Tyr-OH series, with several of the main absorption peaks assigned. The O−H and C−O stretches are essentially unchanged relative to Tyr-

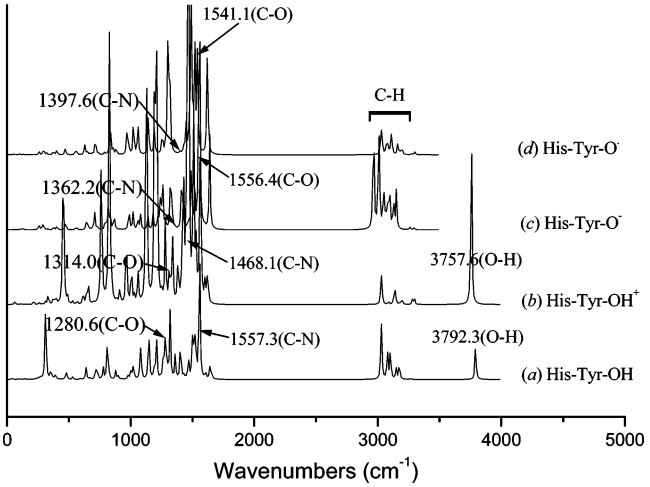

Figure 8. IR spectra of the His-Tyr-OH series derivatives and some special vibrational modes.

OH, in agreement with the bond length changes. Note that a new strong absorption peak appears at 1557 cm^{-1}, which corresponds to the C−N stretch, and this value also implies the double-bond character of the C−N bond. Recently, Tomson et al. also performed direct IR detection of the covalently ring-linked His-Tyr structure in the active site of the heme−copper oxidase using a synthetic analogue, and a special spectroscopic signature near 1546 cm^{-1} was observed and assigned to the C−N stretching vibration.[16] Our predicted C−N frequency is very close to Tomson's value.

For the cross-linked system, upon electron ionization to form the His-Tyr-OH^+ radical cation, the C−O bond is reduced by only 0.024 Å, smaller than the change in the unsubstituted case, and the O−H bond is also basically unchanged. The overall changes for the C−C bonds in the His-coupled Tyr systems are smaller than that in the uncoupled one. Comparison of the His moiety indicates a significant change in the imidazole ring geometries, and the delocalized π bonding on the imidazole ring tends to be more localized. The charge distribution change is significantly different from that in the Tyr-OH/Tyr-OH^+ system. The ionized electron is 53% from the His moiety and 47% from the Tyr moiety. As mentioned above, for the His-Tyr-OH species, the His moiety carries 0.326*e* positive charge, indicating His to be a donating electron group. Thus, both the single electron ionization and the electron transfer from His to Tyr moieties lead to the single electron distribution mainly over the His moiety (86%). The −OH group charge is basically unchanged, indicating that it still keeps the nature of −OH in Tyr (before oxidation). The same is true for the phenyl ring. The spin density analysis also indicates an interesting change compared with that in Tyr-OH^+. The spin density over the imidazole ring is 64%, while that over the phenyl ring is only ∼34%. However, the distribution over −OH is 6%, basically equivalent to that in Tyr-OH^+. The above analysis shows that the ionized electron is taken mainly from the imidazole ring.

Figure 8 presents the IR spectral changes due to the oxidation His-Tyr-OH → His-Tyr-OH^+. The O−H stretching peak is red-shifted by 35 cm^{-1}, but the C−O stretching peak is blue-shifted by 34 cm^{-1}. The trend is the same as that in the Tyr-OH/Tyr-OH^+ case, with the differences attributable to the covalent linkage of His to Tyr. Another strong absorption peak originates from the C−N stretching vibration, and the red shift upon oxidation is ∼90 cm^{-1}. More interesting is that the IR shift is not in agreement with the corresponding bond length change; rather, it follows the decrease of the aromaticity of the imidazole ring and the change in conjugation.

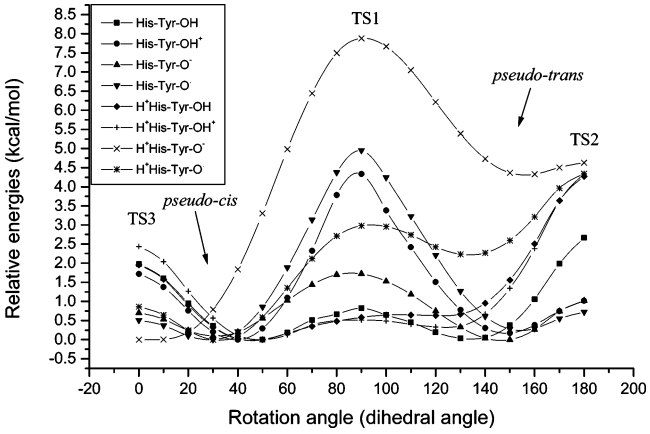

Figure 9. Relative rotation potential surfaces of the His-Tyr-OH series derivatives and H^+His-Tyr-OH series derivatives with respect to the dihedral angle (∠C1C2N7C8) around the linking bond (C2−N7). The zero point for each species is referred to its most stable geometry (the corresponding pseudo-cis rotamer). TS1 denotes the transition state of the rotation isomerization between the pseudo-cis and pseudo-trans rotamers. TS2 and TS3 denote those between the corresponding image rotamers.

Upon deprotonation to His-Tyr-O•, the C−O bond length is further reduced by 0.11−1.246 Å. The data in Figure 2 show that the His substitution has considerably affected the geometrical structure of both the phenyl and imidazole rings. Since the −OH proton is removed, decreasing the ability to withdraw electron density from the phenol moiety, a large part of the electron cloud (0.53*e*) moves to the imidazole ring. Similarly, the spin density distribution over the imidazole ring basically becomes zero, mostly transferring to the phenyl ring *ortho*- and *para*-C sites and the O center (cf. Figure 6). Examination of Figure 6 shows how the spin density changes before and after −OH proton release and contrasts the His-Tyr-OH^+/His-Tyr-O• and Tyr-OH^+/Tyr-O• systems.

The ionization potential IP1 = 172.21 kcal/mol for His-Tyr-OH → His-Tyr-OH^+ (Figure 3) is considerably smaller than the 182.8 kcal/mol value for Tyr-OH → Tyr-OH^+, implying a significant His substituent effect. More interesting is that the IP1 value of His-Tyr-OH is also considerably smaller than the IP (191.0 kcal/mol) of the methyl-substituted imidazole molecule (modeling His). Thus, the covalent coupling between His and Tyr moieties significantly decreases the IP of the His moiety. Also, after electron transfer, proton release becomes easier. The corresponding proton dissociation energy (PD2) is 222.1 kcal/mol, significantly smaller than the 337.0 kcal/mol value before electron ionization. It is slightly larger, by 8 kcal/mol, than that (214.8 kcal/mol) in the Tyr-OH situation, indicating that the coupling interaction from His slightly increases the proton release energy. This observation is in agreement with the analysis about the charge transfer between phenol and imidazole rings, confirming that the Tyr group is the electron donating group.

The dihedral angle between the two ring planes becomes ∼29° after the proton release, ∼11° smaller than those of His-Tyr-OH and His-Tyr-OH^+. The proton release reduces the steric repulsion between the OH and the one C−H group of the imidazole ring. As a result, the conjugation degree between the two rings increases. Figure 9 displays the rotation surfaces around the C−N linkage. Similarly, the dihedral angle between the two rings in the pseudo-trans rotamer is enlarged. The rotation barrier between the pseudo-cis and pseudo-trans rotamers is increased by ∼1.0 kcal/mol, but the image tautomer isomerization barriers are slightly lowered. For this radical

system, the *cis*/*trans* rotation isomerization barrier is increased and the image rotation barriers are slightly lower than the corresponding ones of His-Tyr-OH. A recent theoretical investigation[27] at a lower level of theory (B3LYP/3-21G*) predicted that His-Tyr-O$^{\bullet}$ for both cis and trans isomers are conjugated planar structures. Our pseudo-cis and pseudo-trans geometries are only 0.5 kcal/mol more stable than the corresponding cis and trans ones.

For the anion intermediate His-Tyr-O$^-$, the geometry of the phenol moiety is very similar to that in Tyr-O$^-$, and the geometry of the imidazole moiety is also basically the same as that of the methyl-substituted imidazole molecule. The charge transfer is almost equal to zero, considerably smaller than that (0.33*e* from imidazole ring to phenol ring) in the His-Tyr-OH species. The linking C−N bond increases from 1.419 to 1.433 Å, indicating a decrease in coupling strength change between the two rings. The IR spectra in Figure 8 also show a similar regularity. Besides the disappearance of the O−H stretching vibrational peak, the C−N linking bond is red-shifted by 195 cm^{-1}, and the C−O stretching peak is blue-shifted by 276 cm^{-1}, compared with the His-Tyr-OH molecule.

A comparison of IP1 and PD1 between His-Tyr-OH and Tyr-OH indicates that the His coupling effect decreases both IP1 and PD1 of the Tyr moiety. When electron transfer is prior to proton transfer, the imidazole ring may provide electrons to the phenyl to enhance the aromaticity of the phenyl ring. However, when proton transfer is first, the imidazole ring could accept electron density from the phenyl ring, which has a denser negative charge population.

Imino-N-Site-Protonated Cross-Linked Histidine-Tyrosine. In this section, a proton is attached to the imino N site, forming H$^+$His-Tyr-OH. From the series of derivatives, we can extract the cation charge effect on the structural, energetic, and spectroscopic properties. Since the N site is ligated to a monovalent metal cation, Cu_B, in the fully reduced and partially oxidized states in C*c*O, we use a proton to model the effects from the monocation.

H$^+$His-Tyr-OH. Figure 2 shows the geometry of the H$^+$His-Tyr-OH species. Comparison with that of the unprotonated system indicates that the protonation does not produce a significant effect on the geometrical parameters of the phenol moiety, and the same is true for the imidazole fragment except for two C−N bond lengths (C8−N7 and C8−N9) associated with the [−N7−C8−N9−] part of the imidazole ring in which two C−N bonds tend to the averaged ones (from 1.374/1.309 to 1.334/1.340 Å). Another change is the C−N linkage, which is elongated from 1.419 to 1.439 Å, indicating that the proton coupling interaction to the imino N9 site weakens the linking bonding. This also implies the cation coupling effect on the C−N linkage. Comparison with the geometry of the protonated methyl-substituted imidazole molecule (H$^+$His, the modeling His) also demonstrates their structural similarity. The IR spectra in Figure 10 also display a different character from that in Figure 8 for the His-Tyr-OH species. The O−H and C−O stretches of the phenol moiety are almost unchanged compared with those of the unprotonated situation, but there is a red shift of the C−N linking bond stretch and the appearance of one strong N−H stretch at 3627 cm^{-1}. The red shift, ∼210 cm^{-1}, also indicates the weakening of the C−N linkage bond. These observations are in good agreement with the geometrical changes.

Figure 9 displays the rotational isomerization surface. For His-Tyr-OH species, it is basically symmetric relative to a rotation angle of 90°, but the approximate symmetry is broken after the imino N9 site protonation, though the change is modest.

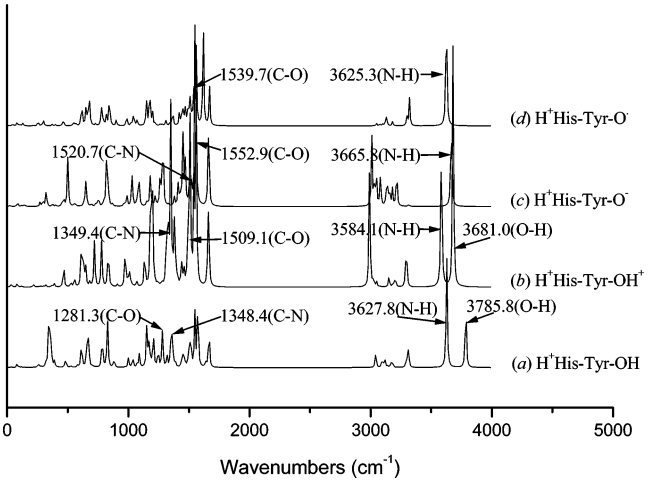

Figure 10. IR spectra of the H$^+$His-Tyr-OH series derivatives and some special vibrational modes.

When the rotation angle is smaller than 100°, the surface is basically unchanged, but then, it becomes shallower. The dihedral angles for the pseudo-cis and the pseudo-trans rotamers are essentially unchanged; the pseudo-cis/trans isomerization barrier is slightly reduced, and the image pseudo-cis/trans isomerization is slightly enlarged.

These changes may be related to the charge repopulation. For the protonated system, the overall charge over the phenol moiety is −0.15*e*, smaller by 0.18*e* than that in the unprotonated system. The overall net charge over the imidazole ring is about 1.15*e*, indicating that the additional positive charge is basically located on the imidazole ring.

H$^+$His-Tyr-OH$^+$. In the H$^+$His-Tyr-OH$^+$ radical cation, the ionized electron comes mainly (78%) from the Tyr moiety. The His fragment carries 1.368*e* positive charge, implying that the His moiety may be viewed as the protonated one. An interesting difference relative to His-Tyr-OH is the spin density change. The spin density for H$^+$His-Tyr-OH$^+$ mainly distributes over the O center (16%), the C1 (═O) center (24%), the *ortho*-C (C2) linked to the imidazole ring (12%), and *para*-C (38%), whereby ∼90% is over the whole phenol ring, but that for the unprotonated case has more than 50% over the imidazole ring (cf. Figure 6).

There are small changes in geometry upon electron ionization. The dihedral angle between the two aromatic planes slightly increases (∼4°) for the pseudo-cis rotamer. The direction of variation is inverse to that in the His-Tyr-OH/His-Tyr-OH$^+$ situation, implying a reduction in conjugation between the two aromatic planes. As occurred in its neutral form, the stability difference between the pseudo-cis and pseudo-trans rotamers increases. The barrier of the isomerization between the pseudo-cis and pseudo-trans structures is even lower, and the image ones increase slightly. Thus, the cation coupling at the imino N9 site slightly increases the rotation ability around the linking C−N bond.

Electron ionization red shifts the N−H and the O−H stretches by 43 cm^{-1} and 104 cm^{-1}, respectively, and the O−H peak is also red-shifted relative to that of His-Tyr-OH$^+$, by 76 cm^{-1}. For the His-Tyr-OH system, upon electron ionization, the C−O absorption peak shifts a little, and the C−N mode shifts slightly more (∼90 cm^{-1}). However, for the H$^+$His-Tyr-OH system, Figure 8 indicates that electron ionization produces a C−O stretch blue shift (228 cm^{-1}), but the C−N mode is basically unshifted. The cation coupling at the imino N9 site of the imidazole ring can regulate the structural property of the active center tyrosine species.

H^+His-Tyr-O•. After proton release to form H^+His-Tyr-O•, the C−O bond length is further reduced to 1.245 Å, a C═O double bond. The C−C and C−N bond lengths change minimally, and the geometry of the imidazole ring is almost unchanged. The dihedral angle decreases to 33°, smaller by 16° than before proton release. The rotation surface becomes more asymmetric, with the pseudo-cis rotamer stability increasing relative to the pseudo-trans rotamer and the barrier between them also increasing (see Figure 9).

In the IR spectra, the H−O peak disappears, and both the N−H and C−O modes are slightly blue-shifted by 30−40 cm^{-1}, respectively. The C−N stretching is basically unchanged, but the strength is reduced. Upon proton release, a part of the charge transfers back to the imidazole moiety, making the Tyr fragment essentially neutral and the His fragment as the protonated one. For the spin density, although it is also almost all over the Tyr moiety, the distribution has changed significantly compared with that in H^+His-Tyr-OH^+ (cf. Figure 6). The distribution is mainly over the O center and the *ortho*-/*para*-C site (C2/C6, C4), very similar to that in the Tyr-O• case and significantly different from that in the His-Tyr-O• case.

For H^+His-Tyr-OH (cf. Figure 3), IP1 is 261.7 kcal/mol, and the further proton release energy (PD2) is 137.6 kcal/mol. Comparison with the unprotonated systems reveals that IP1 increases by ∼90 kcal/mol and PD2 decreases by ∼85 kcal/mol. Thus, cation coupling at the imino N9 site significantly inhibits electron ionization and promotes −OH proton release, implying a charge regulation role in the electron/proton transfer processes. For this protonated system, PD1 is calculated to be 259.8 kcal/mol, smaller than that for His-Tyr-OH by ∼77 kcal/mol. In H^+His-Tyr-OH, PD1 is slightly smaller than IP1, implying that electron ionization becomes competitive with the proton release when a cation is attached to the imino N9 site. The calculated IP2 value (139.4 kcal/mol), slightly larger than the PD2 value (137.6 kcal/mol), also supports this analysis. Therefore, it may be predicted that the relative priority of the electron/proton transfers may be regulated by changing the charge amount coupling to the imino N9 site.

H^+His-Tyr-O^-. The positive charge coupling to the imidazole increases the possibility of proton release relative to electron ionization, making the anion mechanism more probable. In this species, the C−O bond length is significantly reduced to be a double bond. All C−C bonds in H^+His-Tyr-O^- are similar to those in His-Tyr-O^-, the unprotonated one, and the C−N bond is shortened by 0.011 Å. Proton release strengthens the conjugation between O and its linked C center (C1). As a result, the neighboring C−C bonds (C1−C2/C1−C6) are reduced, and the imidazole ring bond lengths also slightly change. The greatest change lies in the dihedral angle between the two ring planes, being decreased by 40°, to make them close to coplanar. Obviously, this geometry is favorable to the formation of a superconjugated big π bond system. The pseudo-trans dihedral angle is ∼155°, larger than those of the pseudo-trans rotamers of the proton-unreleased systems. The energy difference between the pseudo-cis and the pseudo-trans rotamers becomes larger, and the pseudo-cis/pseudo-trans barrier is notably increased, but the image barriers are decreased. The increased rotational barrier may be attributed to the breaking of the superconjugated big π bond system. The proton release causes negative charge transfer of ∼0.44*e* from the tyrosinate fragment to the histidinium. The IR spectra also display significant blue shifts for the C−N and C−O bonds, implying strengthening of these bonds.

Point Charge Effect on Charge/Spin Distribution and Energy Quantities. As found above, protonating the imino N site (N9 site) of the imidazole ring has a significant effect on the charge population and spin density distribution, and on the electron ionization potential and the proton release energy of the Tyr moiety. For C*c*O, the positive charge attached to that N site may vary subject to the stage of the redox process. Because of the coordination interaction of the aromatic imidazole rings, the effective positive charge over the Cu_B center should be in the range from 0 to +1 instead of just +1, corresponding to an effective coupling charge to the imino N site in the same range. For the fully reduced and partially oxidized states, +1 should be the upper limit of the effective positive charge. Thus, in this subsection, a point charge model is used to examine the effect of positive charge ranging from 0 to 1 on the IP, PD, charge population, and spin density distribution over the Tyr fragment.

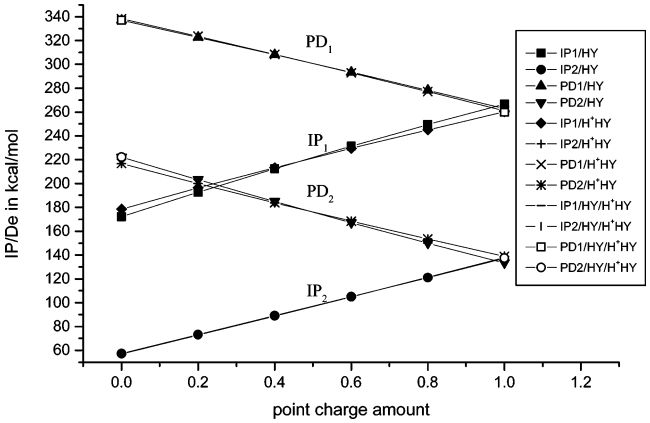

Figure 11. Point charge amount dependencies of IP and PD described in Figure 1 for His-Tyr-OH derivatives. IP1/HY means that the results are calculated at the corresponding His-Tyr-OH derivative geometries, while IP1/H^+HY means that they are calculated at the corresponding H^+His-Tyr-OH derivative geometries. IP1/HY/H^+HY denote the results for the His-Tyr-OH series and H^+His-Tyr-OH series, instead of the point charge model results. The same is true for other quantities (IP2, PD1, and PD2).

On the basis of the optimized geometries of the H^+His-Tyr-OH series, a point charge is placed at the proton position with the same distance as that in the protonated species. The point charge ranges from 0 to +1 in steps of 0.2. Just single point calculations have been done, instead of including the geometrical deformation contributions. To evaluate a part of geometrical deformation energy contributions, the same has been done for the unprotonated His-Tyr-OH geometries. The dependences of four energy quantities, the charge population, and the spin density distribution on the point charge amount are given in Figures 11−14, respectively. The protonated and unprotonated IP and PD lines are consistent with each other, indicating that the geometrical deformation effect caused by attaching an excess positive charge at the imino N site is small. To compare the point charge model results with those of the protonated and unprotonated situations, the corresponding IP and PD values are displayed in Figure 11 (the last four in the symbol remark box). They also exhibit good agreement with those calculated using the point charge model, implying that the electrostatic interaction occurring from the positively charged groups plays the main role in affecting the IPs and PDs. Figure 11 shows an excellent linear relationship between the energy quantities and the effective positive charge amount. In the lower positive charge zone, where PD1 is greater than IP1, electron release is more preferable than proton release, but around +1, the two lines essentially cross. The corresponding energy quantities of their successive processes, PD2 and IP2, also tend to be

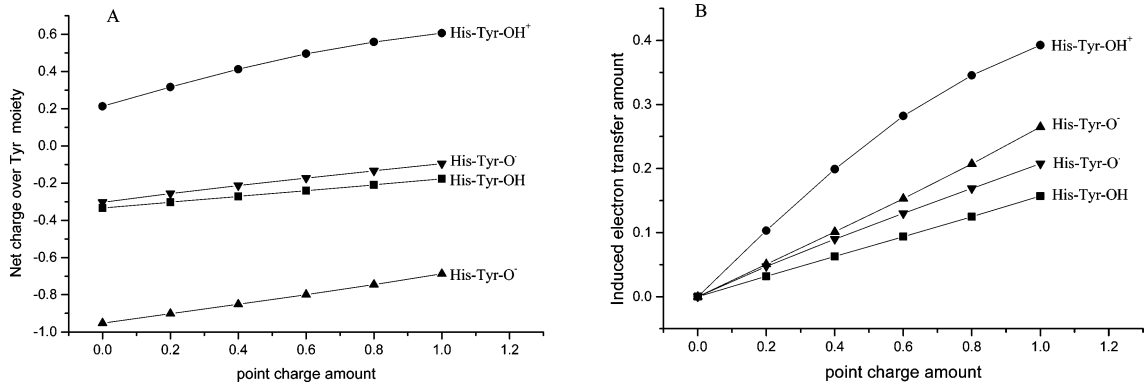

Figure 12. Point charge amount dependencies of the net charge populations (A) over the Tyr moiety and the induced electron transfer amounts (B) from the Tyr moiety for four His-Tyr-OH derivatives obtained at the corresponding H^+His-Tyr-OH derivative geometries by replacing H^+ with the point charge.

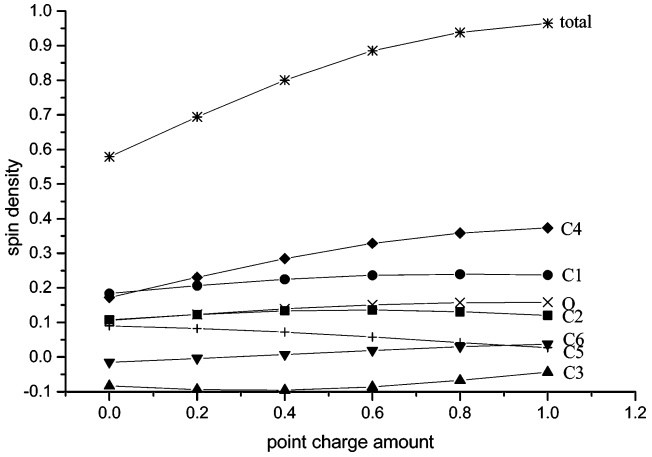

Figure 13. Point charge amount dependence of the spin density over different atomic centers and total spin density of the Tyr moiety in the His-Tyr-OH^+ radical cation calculated at the H^+His-Tyr-OH^+ geometry.

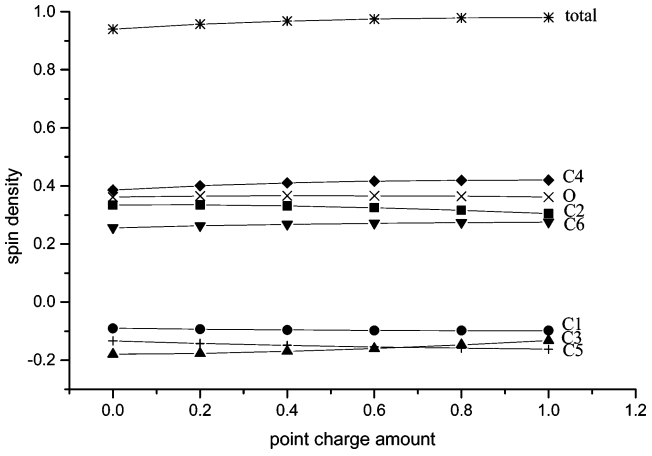

Figure 14. Point charge amount dependence of the spin density over different atomic centers and total spin density of the Tyr moiety in the His-Tyr-O$^\bullet$ radical calculated at the H^+His-Tyr-O$^\bullet$ geometry.

comparable. Roughly speaking, without considering the structural character of the acceptors to which the released electron/proton will move, a changeover in character of electron versus proton release occurs around +1 valence charge.

Figure 12 gives the dependences of the charge populations and the spin densities on the point charge amount for the His-Tyr-OH series, at the corresponding H^+His-Tyr-OH series geometries. As found in the comparison between His-Tyr-OH^+/His-Tyr-O$^\bullet$ and H^+His-Tyr-OH^+/H^+His-Tyr-O$^\bullet$, the positive charge electrostatic interaction produces significant effects on these electronic distribution indexes. For the charge population, since His and Tyr moieties are two aromatic molecular fragments and their frontier orbitals are π-type molecular orbitals, the charge exchange amount directly influences their own aromatic stabilities, and also their IPs and PDs. Therefore, we focus on the electron transfer between the His and Tyr molecular fragments as the point charge amount changes. The electron transfer from Tyr to His moieties increases gradually for the neutral and radical systems, but more rapidly for the two charged species, with increasing point charge amount.

Figures 13 and 14 display the point charge amount dependences of the spin density distributions over several phenyl C and O centers of the Tyr moieties for His-Tyr-OH^+ and His-Tyr-O systems. For the radical cation, C4 and C5 show a modest increase and decrease, respectively, and the others are essentially unchanged. The total spin density over the phenoxy (see "total" curve in Figure 13) significantly increases as the positive charge amount increases. This observation agrees with the spin density change between the His-Tyr-OH^+ and H^+His-Tyr-OH^+ species, revealing the spin density transfer from His to Tyr moieties. For the neutral radical, the spin densities are almost constant with increasing positive charge. The total spin density over the Tyr moiety is greater than 96% in the whole range of positive charge. Thus, the radical cation and neutral radical are quite different in this property.

4. Discussion

Overall Analysis of the Substituent Effect on Relevant Quantities. It is clear from the above analysis that the properties of the Tyr moiety strongly depend on the nature of the ortho-site-linked group. Figures 2, 4, and 5 summarize the dependence of the energy quantities IP1, PD2, PD1, and IP2, charge populations, and spin densities of the Tyr moiety (a redox center), with the substituents, H-, His-, and H^+His groups covalently linked to the ortho site of the phenol −OH, for the four derivatives.

Compared with Tyr, the His substitution slightly decreases IP1 and PD1, and slightly increases PD2 and IP2. This is in agreement with the experimental findings, by CW-EPR and NMR spectroscopies and so forth,[27] that the imidazole substituent has only a minor effect on the electronic structure of the substituted phenol radical. However, if the *ortho*-H is replaced by the protonated His group, IP1 increases and PD1 decreases to such a degree that they become almost equal, implying that electron transfer and proton release become competitive. Since the protonated His substituent is closer to the actual situation in C*c*O, the cationized His substituent properties are of great

interest. Naturally, the substituent effects on the energy quantities are due to the charge population changes. The dependencies of charge populations on the substituents are given in Figure 4. The neutral and radical species Tyr charge populations are basically independent of the substituent. For the radical cation, the electron density over the Tyr moiety always increases, and for the anion, it always decreases, for all substituents. For the cation radical, the increment of electron population caused by the H^+His group is smaller than that caused by the His group, while for the negative charge decrement in the anion case, the substituent effect of the H^+His group is larger than that of the His group.

The substituents also considerably affect the spin density distributions over the Tyr moiety, as is clear from Figure 6. Not only are the distributions of the radical cation and pure radical different, but also the changes caused by introducing substituents to the ortho site are different. In particular, for the R-Tyr-OH^+ (R═H—, His- and H^+His-) forms, the distribution regularities are almost the same for Tyr-OH^+ and H^+His-Tyr-OH^+, showing that the introduction of H^+His basically does not change the distribution, but for His-Tyr-OH^+, the distribution significantly transfers from Tyr to His moieties. However, for the three radical forms (R-Tyr-$O^\bullet$), the substitutions hardly affect the spin density distributions, so that the spin density is always distributed over the Tyr moiety. Thus, if the Tyr moiety completely loses an electron and proton to form a radical, its spin density distribution is independent of ortho site substitution, and the spectroscopic signal should be invariant. However, if the released proton is not completely away from the O center upon the electron ionization, the spin density will depend on not only the position of the released proton but also the nature of the substituent. The distributions are mainly over the ortho and para site of the phenoxy radical, but protonation of the O center transfers spin density from the unsubstituted ortho site (C6) to the (O═)C1 site, and the spin density distribution is also sensitive to the substituent. These differences may provide useful information for experimentally determining the binuclear center structure, and how it changes in the redox process. Of course, if the released proton is H-bonded back to the O center, the effect from the feedback H-bond is smaller than that from the direct protonation of the O center; thus, the spin density distribution would be between that of the radical cation and the radical, but closer to the radical case.

Recently, two groups reported the synthesis and spectroscopic characterization of the modeling cross-linked histidine-tyrosine molecule (His-Tyr-OH).[26,27] In particular, Britt's group, in addition to the CW-EPR, ESEEM, and NMR investigations, also scanned the rotation potential surfaces by changing the dihedral angle between the phenol and imidazole rings and relaxing all other geometrical parameters at the B3LYP level with a small basis set (3-21G*) and predicted that the pseudo-cis rotamer is slightly more stable than the pseudo-trans rotamer, with an energy difference of 0.08 kcal/mol, in agreement with our result. They also discussed the radical His-Tyr-$O^\bullet$ but not the intermediates, His-Tyr-OH^+ and His-Tyr-O^-.

The spin density distributions shown in Figure 6 provide a way of deciding whether electron and proton transfer (in either order) may be viewed as H-atom transfer. All three paths lead to the same product and, as shown above, result in major electronic structural reorganization. Clearly, the reaction is not a simple O−H bond cleavage and then H-atom transfer. If so, the radical formed should correspond to $-O^\bullet$; namely, the spin single electron should be at the O center instead of largely over the phenyl ring. Furthermore, the negative charge population over the O center is only −0.2 to −0.3*e*, and the electron removal is mainly from the phenyl ring. Even if the released proton and electron may be viewed as a H atom donated to the acceptor center, they do come from different parts of the Tyr moiety. Therefore, this proton/electron transfer process cannot be described as a simple H-atom transfer. Perhaps, it is appropriate to be described as a proton-coupled electron transfer process or an electron-coupled proton transfer process. Of course, for the inverse (recovery) process for the next cycle of the O_2 reduction, the requisite electron and proton come from different parts of C*c*O. Here, clearly, the process must be described as concerted or consecutive electron/proton transfer, instead of H-atom transfer. These considerations emphasize that it is essential to explore the energetics of the four species we define, and characterize them in regard to their structural and spectroscopic signatures.

The effect of substituents on the Tyr properties can be quite large. When Tyr is covalently linked by a His group, its structural character and electronic properties change significantly. These observations are different from the findings by Kim et al. in which they predicted no significant change for the structural property of Tyr covalently linked by His. In this work, we have found that the Tyr properties are more similar in the system covalently linked by a H^+His group instead of a His group. The similarity between Tyr series and H^+His-Tyr series in structural changes, IR changes, and energy properties is good evidence for our predictions.

Biological Implications. In a number of redox enzymes, such as ribonucleotide reductase,[47,48] prostaglandin H synthase,[49,50] and photosystem II (PSII),[51,52] the Tyr radical is known to play a crucial role. In view of their importance, model systems for them have been designed and extensively studied.[53−58] However, a covalent linkage of Tyr with His has only been observed in C*c*O, and this unusual linkage may have novel properties. That the Tyr may occur as a radical in C*c*O has been suggested by experiments that detected a radical EPR signal following reaction with hydrogen peroxide.[13,59,60] This EPR signal was alternatively identified as arising from a tyrosine[13] and a tryptophan radical.[59] More recently, evidence was also reported suggesting that the cross-linked His-Tyr is oxidized to a radical form.[12] The concerted electron and proton transfer from this special cross-linked structure could provide an additional impetus for the O−O bond cleavage and/or energy conduction by proton translocation. While these assignments still remain to be confirmed by direct spectroscopic observation of the proposed His-Tyr radical, the mechanistic aspects of this proposal regarding the formation of the His-Tyr radical are appealing, and this motivated our efforts to determine the electronic structure of such cross-linked His-Tyr radicals.

As an appropriate model to mimic the cross-linked His-Tyr in C*c*O, we use *para*-cresol crossed-linked by methyl-imidazole, with the possibility of protonating its imino N site. Since, in C*c*O, the cross-linked His is ligated to the Cu_B center, protonation of the imino N site of the ligand His can serve as a model for the metal. As shown in several recent studies,[7,14,15,17,21,26,61] the cross-linking with His may act to alter the oxidation potential or pK_a of the Tyr. No previous investigation has studied the relative priority of electron ionization and proton delivery after perturbation from the modeling His or from protonated His. These perturbations will modulate the concerted or separated electron/proton transfer mechanism. Although our calculated lowering of the IP1 (∼10 kcal/mol) and PD1 (∼13 kcal/mol) values compared with His-unlinked modeling Tyr show an effect from the cross-linking His substituent, since PD1

is still significantly larger than IP1 by ~165 kcal/mol, electron ionization is still preferred much more than proton delivery. Even if one electron is first transferred, the following proton dissociation still needs considerable energy (PD2 = 222.1 kcal/mol), which is also significantly larger than the electron ionization energy (IP1 = 172.2 kcal/mol). Thus, if only a His is cross-linked to Tyr, the inherent nature of the Tyr ensures the electron transfer priority. Indeed, as mentioned above, this analysis also implies the improbability of H-atom transfer, because the direct H-atom transfer from the Tyr moiety to the terminal O of dioxygen is energetically unfavorable, even if it is in hydrated form, due to the large distance (~5 Å) between the Tyr O and the terminal O.

When the imino N site is protonated, the relative release priority between the electron and the proton is drastically modified. As noted above, since the imino N9 site of the imidazole ring of His that is covalently linked to Tyr lies in a variable positive charge surrounding (between $Cu(I)L_2$ and $Cu(II)L_2$, L = histidine), the actual valent state or charge change of the Cu_B center may regulate the priority of electron/proton transfer from the Tyr moiety. Also, the vibrations of the coordination bonds, and other motions, probably change the structural characteristics, such as the distance between the Cu center and the imino N of His covalently linked with Tyr. As a result, the effective positive charge may change following the geometrical changes of the Cu_B center, making the charge scan calculation carried out a useful procedure to represent the consequence of these changes. The data shown in Figure 11 summarize the charge scan and the H^+His-Tyr-OH series results. They show that, as the charge is increased to +1, IP1 increases and PD1 decreases to such an extent that the energetics of the two processes are almost equivalent, even slightly favoring proton transfer. Note that the H^+His-Tyr-OH series agrees well with the +1 limit of the charge scan, indicating a strong electrostatic effect. Therefore, for both oxidation of Tyr and the corresponding reduction process of the Tyr radical, proton and electron transfer become competitive, and the two transfers may be cooperative. Since the coupling interaction with and the effective positive charge over the Cu_B center may vary as the reaction proceeds, this positive charge effect may be viewed as a factor that modulates the inherent redox reactivity of the Tyr redox reaction center.

Actually, it is the case in C*c*O that the electron transfer from the Cu center to dioxygen is probably prior to that from the Tyr moiety, resulting in the valence state of the Cu center higher than +1. However, the O−O rupture mechanism that is generally proposed asserts that, upon receiving the third electron from the Cu center, the O−O bond is broken, and then, the terminal O atom may move to the Cu center as an OH^- ligand, by binding an external (chemical) proton. Therefore, even if Cu behaves as a dication, the effective positive charge over the Cu center is perhaps not larger than +1 due to the neutralization from the OH^- anion ligand.

The changes of charge population and spin density distribution over the Tyr and His moieties compared with those in the imino N unprotonated situation also strongly support a modulation role for the His fragment via the cross-linkage to the Tyr fragment. For the neutral species (the Tyr and Tyr radical groups), the charge populations over the Tyr moieties in the protonated and unprotonated cases are not notably different, implying that the charge transfer induced by H^+ attachment to the imino N site is small. However, for the Tyr cation radical and the Tyr anion (the intermediates or metastable species), the charge populations change considerably from the cation effect. For the anion case, the positive charge and modeling His substituent produce a cooperative contribution to the charge population over the Tyr moiety. Namely, the imidazole ring substituent decreases the negative charge density over the Tyr moiety, implying considerable charge transfer from the Tyr to His moieties, and the positive charge attachment at the imino N site further enhances the charge transfer. For the radical cation species, the inverse trend is observed. Introduction of the modeling His substituent decreases the positive charge population over the Tyr moiety, and cationization at the imino N site decreases the His substituent effect on the positive charge population over the Tyr part.

These observations indicate that the linked imidazole ring may be viewed as an electron cloud buffer. In the anion cases (R-Tyr-O^-), the imidazole ring may store electrons coming from the Tyr moiety, dispersing the negative charge over the Tyr to the His while, in the radical cation, donating electrons to the Tyr moiety and dispersing the positive charge over the Tyr to the His. Thus, protonation or cationization of the imino N site may act as a regulator, playing different roles in modulating the charge transfer amount between Tyr and His moieties. Namely, for the anion, it enhances the ability of storing electrons of the imidazole ring, but for the cation radical, it decreases the imidazole ring's ability to donate electrons. This indicates that the possible species produced in the intermediate processes are sensitive to the charge effect; thus, it provides a basis for regulation. Again, because the transferred proton may be H-bonded back to the Tyr O center, the radical and the protonated radical cases may be viewed as two limits of a continuum.

Similarly, the spin density distributions support modulation of functionality by the linked His and the cationization effects. For the pure radical without any effect arising from the surroundings, the introduction of the His substituent into the ortho site of the Tyr moiety does not significantly change the spin density distribution over the Tyr moiety (dispersing only about 10% to the imidazole ring), and further attachment of an imino N site cation reduces the dispersion (cf. Figure 6). However, if an excess proton that is to be used to reprotonate the radical is H-bonded to or strongly coupled with the Tyr O center, the spin density distribution depends strongly on the presence of the His substituent and its protonated version. However, for the radical cation, the introduction of a His substituent significantly disperses the spin density from the Tyr to the His, and cationization of the His significantly counteracts this dispersing effect (cf. Figure 6). These results are considerably different from those found in the model Tyr radical species in this work and others,[27] indicating the sensitivity of the spin density distribution to the surrounding effect.

The anion mechanism that first has proton transfer may be favored in C*c*O based on the following considerations. After dioxygen is diffused into the heme a_3 Fe center, two electrons come from the Fe center to reduce Fe(II)−O_2 to Fe(IV)−O^-−O^-. Consequently, there is a larger electron cloud density over the terminal O center, resulting in a stronger ability to accept the incoming proton. Thus, there is a greater possibility of releasing a proton before electron transfer for the phenol fragment. Assuming that the third electron comes from the Cu_B center, this transfer will increase the negative charge over the O_2 terminal oxygen, thereby not only increasing the proton withdrawing ability but also possibly breaking the O−O bond. These features make the anion mechanism more probable. Although no experimental evidence for this prediction has been

reported up to now, it may be due to the short-lived nature of such an anion.

Together with IP and PD energy factors, all of these observed phenomena strongly imply that the cation effect may considerably change the relative priority of the proton release and the electron release, the charge population, and the spin density distribution of relevant species possibly occurring in the O_2 reduction reaction even if it has a +1 valence state. Therefore, it may be predicted that, in the oxidative half reaction, a reasonable mechanism for proton/electron release from the Tyr moiety should be that the proton release is prior to the electron release and, even if they are coupled together, the proton release should be dominant. The charge exchange between Tyr and His moieties also suggests the possibility that the electron release may utilize the Tyr → His → Cu(II) → O−O$^-$ pathway instead of the direct transfer via Tyr → O−O$^-$. Of course, in the recovery process, the electron affinity of the Tyr radical is larger than the proton affinity, so that electron transfer should be first. These predictions still need further confirmation by taking the properties of the Cu_B center, heme a_3, and the surrounding residues into account, and the relevant calculations are underway.

5. Concluding Remarks

In this work, structural, energetic, and electronic and IR spectroscopic properties have been investigated for a model cross-linked His-Tyr and their relevant derivatives. Methyls are used to mimic the Tyr and His side chains by appropriately bonding them to phenol and imidazole, respectively. The His and Tyr models are cross-linked via the ortho site of the modeling Tyr and the amino N site of the modeling His, as occurs in C*c*O. In view of their functional roles in C*c*O, two schemes are designed for the proton and electron releases from the modeling Tyr moiety to form the corresponding radical, namely, the anion mechanism (proton transfer followed by electron transfer) and the radical cation mechanism (electron transfer followed by proton transfer). Several conclusions can be drawn as follows.

(1) The energetics for the proton/electron releases of the Tyr moiety in C*c*O depend not only on the cross-linked His substituent but also more sensitively on the cation effect, from attachment to the imino N site of the His residue. The cross-linkage in the Tyr and His model modestly decreases the PD and IP, and protonation at the imino N site significantly increases the IP (∼90 kcal/mol) and decreases the PD (∼77 kcal/mol), making the IP and PD of the modeling Tyr essentially equivalent. A further increase of positive charge at the imino N site results in an IP greater than the PD. The point charge model we use supports this regularity. The positive charge (+1) may be a criterion by which the priorities of proton and electron release may be altered. The improbability of a direct hydrogen-atom transfer from the Tyr active center to dioxygen has also been shown.

(2) The introduction of the modeling His, or its protonated version, yields different effects on the geometries of the possible stable/metastable species or intermediates and their IR absorption spectroscopies. The geometrical changes from the modeling Tyr to the modeling Tyr radical via two proposed intermediates, the modeling Tyr cation radical and the anion, resulting from introducing the *protonated* modeling His, are basically the same as those of *p*-cresol but differ from those resulting from introducing the modeling His, indicating that the protonated modeling His minimally changes the inherent trends of the Tyr moiety in the redox process but the modeling His has a substantial effect. This observation also reveals the importance of the cation attachment at the imino N site in maintaining the inherent structural change of the Tyr moiety in the cross-linked form, similar to that of the Tyr residue. The corresponding IR spectroscopic signals reflect the structural changes in the redox processes and provide a basis for the detection of the possible intermediate species. The small rotational barriers found separating the pseudo-cis and pseudo-trans rotamers, and the image isomers, demonstrate the relative flexibility between the two rings and, by relaxing the system to an optimal conformation, may facilitate proton release and charge transfer.

(3) The significantly different effects on the charge population and the spin density distribution changes that arise by introducing the protonated and unprotonated modeling His substituents imply a modulation role on the charge transfer between the phenol and imidazole rings. For the neutral species (the modeling Tyr and the corresponding radical), both substituents have a minor effect on the electronic structures, but for the two charged species, their effects are quite different. This modulation role is mainly reflected in the charge transfer and the spin density redistribution between the two rings. Together with the IP and PD changes, these observations suggest that, in the oxidative stage, electron transfer from the Tyr center to dioxygen may be coupled to the preferential proton transfer, but the electron transfer takes place using a different pathway from the proton transfer. The electron transfer pathway may be via the cross-linkage to the Cu_B center and then to the species generated from dioxygen cleavage. Of course, this mechanism needs further evidence.

(4) In view of the effect of the cross-linked His residue and the importance of the cation attachment at the imino N site of the imidazole ring, the cationized cross-linked His-Tyr should be the best candidate to mimic the covalently ring-linked tyrosine-histidine structure in C*c*O.

Finally, it is clear that the proton/electron transfers associated with the dioxygen reduction to water is a complicated process that involves electron and proton transfer and the transition between oxygen intermediates and the binuclear center. In addition to the inherent nature of the modeling cross-linked His-Tyr, the mechanism of the electron and proton transfers from or to the Tyr center also strongly depends on factors such as the properties of O_2 bound to the heme a_3 and Cu_B center, and the H-bond directed to the hydroxyl of Tyr from other groups, or possible water molecules. Further work including these effects is underway.

Acknowledgment. This work is supported by the NIH (Grant No. GM62790). All calculations were carried out on the Center for Biological Modeling and the Michigan Center for Biological Information Linux clusters at Michigan State University.

References and Notes

(1) Wikström, M. K. F. *Nature* **1977**, *266*, 271.
(2) Wikström, M. *Curr. Opin. Struct. Biol.* **1998**, *8*, 480.
(3) Gennis, R. B. *Proc. Natl. Acad. Sci. U.S.A.* **1998**, *95*, 12747.
(4) Michel, H.; Behr, J.; Harrenga, A.; Kannt, A. *Annu. Rev. Biophys. Biomol. Struct.* **1998**, *27*, 329.
(5) Ferguson-Miller, S.; Babcock, G. T. *Chem. Rev.* **1996**, *96*, 2889.
(6) Malmstrom, B. G. *J. Biol. lnorg. Chem.* **1998**, *3*, 339.
(7) Yoshikawa, S.; Shinzawa-Itoh, K.; Nakashima, R.; Yaono, R.; Yamashita, E.; Inoue, N.; Yao, M.; Fei, M. J.; Libeu, C. P.; Mizushima, T.; Yamaguchi, H.; Tomizaki, T.; Tsukihara, T. *Science* **1998**, *280*, 1723.
(8) Ostermeier, C.; Harrenga, A.; Ermler, U.; Michel, H. *Proc. Natl. Acad. Sci. U.S.A.* **1997**, *94*, 10547.
(9) Soulimane, T.; Buse, G.; Bourenkov, G. P.; Bartunik, H. D.; Huber, R.; Than, M. E. *EMBO J.* **2000**, *19*, 1766.

(10) Buse, G.; Soulimane, T.; Dewor, M.; Meyer, H. E.; Bluggel, M. *Protein Sci.* **1999**, *8*, 985.
(11) McCauley, K. M.; Vrtis, J. M.; Dupont, J.; van der Donk, W. A. *J. Am. Chem. Soc.* **2000**, *122*, 2403.
(12) Proshlyakov, D. A.; Pressler, M. A.; DeMaso, C.; Leykam, J. F.; DeWitt, D. L.; Babcock, G. T. *Science* **2000**, *290*, 1588.
(13) MacMillan, F.; Kannt, A.; Behr, J.; Prisner, T.; Michel, H. *Biochemistry* **1999**, *38*, 9179.
(14) Proshlyakov, D. A.; Pressler, M. A.; Babcock, G. T. *Proc. Natl. Acad. Sci. U.S.A.* **1998**, *95*, 8020.
(15) Himo, F.; Noodleman, L.; Blomberg, M. R. A.; Siegbahn, P. E. M. *J. Phys. Chem. A* **2002**, *106*, 8757.
(16) Tomson, F.; Bailey, J. A.; Gennis, R. B.; Unkefer, C. J.; Li, Z. H.; Silks, L. A.; Martinez, R. A.; Donohoe, R. J.; Dyer, R. B.; Woodruff, W. H. *Biochemistry* **2002**, *41*, 14383.
(17) Svensson-Ek, M.; Abramson, J.; Larsson, G.; Tornroth, S.; Brzezinski, P.; Iwata, S. *J. Mol. Biol.* **2002**, *321*, 329.
(18) Moore, D. B.; Martinez, T. J. *J. Phys. Chem. A* **2000**, *104*, 2367.
(19) Wikström, M. *Biochim. Biophys. Acta* **2000**, *1458*, 188.
(20) Vos, M. H.; Lipowski, G.; Lambry, J. C.; Martin, J. L.; Liebl, U. *Biochemistry* **2001**, *40*, 7806.
(21) Aki, M.; Ogura, T.; Naruta, Y.; Le, T. H.; Sato, T.; Kitagawa, T. *J. Phys. Chem. A* **2002**, *106*, 3436.
(22) Kamaraj, K.; Kim, E.; Galliker, B.; Zakharov, L. N.; Rheingold, A. L.; Zuberbuhler, A. D.; Karlin, K. D. *J. Am. Chem. Soc.* **2003**, *125*, 6028.
(23) Siegbahn, P. E. M.; Blomberg, M. R. A.; Blomberg, M. L. *J. Phys. Chem. B* **2003**, *107*, 10946.
(24) Iwaki, M.; Puustinen, A.; Wikstrom, M.; Rich, P. R. *Biochemistry* **2003**, *42*, 8809.
(25) Collman, J. P.; Sunderland, C. J.; Berg, K. E.; Vance, M. A.; Solomon, E. I. *J. Am. Chem. Soc.* **2003**, *125*, 6648.
(26) Cappuccio, J. A.; Ayala, I.; Elliott, G. I.; Szundi, I.; Lewis, J.; Konopelski, J. P.; Barry, B. A.; Einarsdottir, O. *J. Am. Chem. Soc.* **2002**, *124*, 1750.
(27) Kim, S. H.; Aznar, C.; Brynda, M.; Silks, L. A. P.; Michalczyk, R.; Unkefer, C. J.; Woodruff, W. H.; Britt, R. D. *J. Am. Chem. Soc.* **2004**, *126*, 2328.
(28) Cheesman, M. R.; Oganesyan, V. S.; Watmough, N. J.; Butler, C. S.; Thomson, A. J. *J. Am. Chem. Soc.* **2004**, *126*, 4157.
(29) Elliott, G. I.; Konopelski, J. P. *Org. Lett.* **2000**, *2*, 3055.
(30) Blomberg, M. R. A.; Siegbahn, P. E. M.; Babcock, G. T.; Wikstrom, M. *J. Inorg. Biochem.* **2000**, *80*, 261.
(31) Gennis, R. B. *Biochim. Biophys. Acta* **1998**, *1365*, 241.
(32) Sucheta, A.; Szundi, I.; Einarsdottir, O. *Biochemistry* **1998**, *37*, 17905.
(33) Stubbe, J.; van der Donk, W. A. *Chem. Rev.* **1998**, *98*, 705.
(34) Davies, K. J. A.; Delsignore, M. E.; Lin, S. W. *J. Biol. Chem.* **1987**, *262*, 9902.
(35) Curtiss, L. A.; Raghavachari, K.; Redfern, P. C.; Pople, J. A. *J. Chem. Phys.* **2000**, *112*, 7374.
(36) Bu, Y.; Cukier, R. I. *J. Phys. Chem. B* **2004**, *108*, 10089.
(37) Frisch, M. J.; Grucks, G. W.; Schlegel, H. B.; Scuseria, G. E.; Robb, M. A.; Cheeseman, J. R.; Montgomery, J. A.; Vreven, T.; Kudin, K. N.; Burant, J. C.; Millam, J. M.; Iyengar, S. S.; Tomasi, J.; Barone, V.; Mennucci, B.; Cossi, M.; Scalmani, G.; Rega, N.; Petersson, G. A.; Nakatsuji, H.; Hada, M.; Ehara, M.; Toyota, K.; Fukuda, R.; Hasegawa, J.; Ishida, M.; Nakajima, T.; Honda, Y.; Kitao, O.; Nakai, H.; Klene, M.; Li, X.; Knox, J. E.; Hratchian, H. P.; Cross, J. B.; Adamo, C.; Jaramillo, J.; Gomperts, R.; Stratmann, R. E.; Yazyev, O.; Austin, A. J.; Cammi, R.; Pomelli, C.; Ochterski, J. W.; Ayala, P. Y.; Morokuma, K.; Voth, G. A.; Salvador, P.; Dannenberg, J. J.; Zakrzewski, V. G.; Dapprich, S.; Daniels, A. D.; Strain, M. C.; Farkas, O.; Malick, D. K.; Rabuck, A. D.; Raghavachari, K.; Foresman, J. B.; Ortiz, J. V.; Cui, Q.; Baboul, A. G.; Clifford, S.; Cioslowski, J.; Stefanov, B. B.; Liu, G.; Liashenko, A.; Piskorz, P.; Komaromi, I.; Martin, R. L.; Fox, D. J.; Keith, T.; Al-Laham, M. A.; Peng, C. Y.; Nanayakkara, A.; Challacombe, M.; Gill, P. M. W.; Johnson, B.; Chen, W.; Wong, M. W.; Gonzalez, C.; Pople, J. A. *Gaussian 03*, revision B.05 ed.; Gaussian, Inc.: Pittsburgh, PA, 2003.
(38) Bowry, V. W.; Ingold, K. U. *Acc. Chem. Res.* **1999**, *32*, 27.
(39) Sodupe, M.; Oliva, A.; Bertran, J. *J. Phys. Chem. A* **1997**, *101*, 9142.
(40) Re, S.; Osamura, Y. *J. Phys. Chem. A* **1998**, *102*, 3798.
(41) *CRC Handbook of Chemistry and Physics*, 78th ed.; CRC Press: Boca Raton, FL, 1997.
(42) Hartland, G. V.; Henson, B. F.; Venturo, V. A.; Felker, P. M. *J. Phys. Chem.* **1992**, *96*, 1164.
(43) Green, J. H. S.; Harrison, D. J.; Kynaston, W. *Spectrochim. Acta, Part A* **1971**, *27*, 2199.
(44) Tripathi, G. N. R.; Schuler, R. H. *J. Chem. Phys.* **1984**, *81*, 113.
(45) Cabral, B. J. C.; Fonseca, R. G. B.; Simoes, J. A. M. *Chem. Phys. Lett.* **1996**, *258*, 436.
(46) Michalska, D.; Bienko, D. C.; AbkowiczBienko, A. J.; Latajka, Z. *J. Phys. Chem.* **1996**, *100*, 17786.
(47) Larsson, A.; Sjoberg, B. M. *EMBO J.* **1986**, *5*, 2037.
(48) Bollinger, J. M.; Edmondson, D. E.; Huynh, B. H.; Filley, J.; Norton, J. R.; Stubbe, J. *Science* **1991**, *253*, 292.
(49) Karthein, R.; Dietz, R.; Nastainczyk, W.; Ruf, H. H. *Eur. J. Biochem.* **1998**, *171*, 313.
(50) Smith, W. L.; Eling, T. E.; Kulmacz, R. J.; Marnett, L. J.; Tsai, A. L. *Biochemistry* **1992**, *31*, 3.
(51) Barry, B. A.; Eldeeb, M. K.; Sandusky, P. O.; Babcock, G. T. *J. Biol. Chem.* **1990**, *265*, 20139.
(52) Hoganson, C. W.; Babcock, G. T. *Biochemistry* **1992**, *31*, 11874.
(53) Itoh, S.; Taki, M.; Kumei, H.; Takayama, S.; Nagatomo, S.; Kitagawa, T.; Sakurada, N.; Arakawa, R.; Fukuzumi, S. *Inorg. Chem.* **2000**, *39*, 3708.
(54) Halfen, J. A.; Jazdzewski, B. A.; Mahapatra, S.; Berreau, L. M.; Wilkinson, E. C.; Que, L.; Tolman, W. B. *J. Am. Chem. Soc.* **1997**, *119*, 8217.
(55) Wang, Y. D.; DuBois, J. L.; Hedman, B.; Hodgson, K. O.; Stack, T. D. P. *Science* **1998**, *279*, 537.
(56) Chaudhuri, P.; Hess, M.; Muller, J.; Hildenbrand, K.; Bill, E.; Weyhermuller, T.; Wieghardt, K. *J. Am. Chem. Soc.* **1999**, *121*, 9599.
(57) Sokolowski, A.; Muller, J.; Weyhermuller, T.; Schnepf, R.; Hildebrandt, P.; Hildenbrand, K.; Bothe, E.; Wieghardt, K. *J. Am. Chem. Soc.* **1997**, *119*, 8889.
(58) Schnepf, R.; Sokolowski, A.; Muller, J.; Bachler, V.; Wieghardt, K.; Hildebrandt, P. *J. Am. Chem. Soc.* **1998**, *120*, 2352.
(59) Rigby, S. E. J.; Junemann, S.; Rich, P. R.; Heathcote, P. *Biochemistry* **2000**, *39*, 5921.
(60) Fabian, M.; Palmer, G. *Biochemistry* **1995**, *34*, 13802.
(61) Fann, Y. C.; Ahmed, I.; Blackburn, N. J.; Boswell, J. S.; Verkhovskaya, M. L.; Hoffman, B. M.; Wikstrom, M. *Biochemistry* **1995**, *34*, 10245.